Stark effect in nonhydrogenic low-dimensional excitons

Thomas Garm Pedersen ●*

Department of Materials and Production, Aalborg University, DK-9220 Aalborg Øst, Denmark

Excitons in two dimensions and other low-dimensional semiconductors are known to deviate from simple Wannier model descriptions due to nonlocal dielectric screening. As a consequence, energy levels do not follow a simple hydrogenic Rydberg series. Recently, a Kratzer model including a repulsive core potential has been suggested as an analytically solvable model of nonhydrogenic excitons. We adopt this model to describe both static and dynamic Stark effects in low-dimensional semiconductors. An exact formula for the exciton polarizability valid for arbitrary dimension and core potential is obtained. Moreover, analytical oscillator strengths allow for analyses of the dynamic Stark effect in various dimensions and materials.

I. INTRODUCTION

Excitons in low-dimensional semiconductors are a subject of immense interest. They dominate the linear and nonlinear optical response and play crucial roles in light emitting devices and photovoltaics [1–3]. Models of excitons span from highly accurate *ab initio* Bethe-Salpeter equations [4–6] to simplified Wannier descriptions [1–3,7–9]. The former is rather computationally demanding and struggles to incorporate semi-infinite substrates [6] unless screening is introduced via macroscopic dielectric constants [10,11]. In contrast, the latter is exceedingly simple and reduces to a hydrogen atom model if appropriately scaled units are adopted. Thus, in strict two- and three-dimensional cases, analytical eigenstates can be found [1,2]. In fact, using an abstract extension to *D*-dimensional space, analytical eigenstates exist for arbitrary dimensions [12–15]. In turn, this allows for analytical models of optical properties and polarizabilities of *D*-dimensional Wannier excitons [15–17].

The disadvantage of the analytical Wannier model is clearly its limited applicability to actual excitonic states. Thus, while some three-dimensional systems are very accurately described, clear deviations from the Rydberg energy series of hydrogenic models have been found in other three- and, in particular, two-dimensional materials [18–20]. A major ingredient absent in hydrogenic models is position-dependent screening. In fact, Coulomb interactions in freely suspended two-dimensional semiconductors are unscreened at long distances because field lines predominantly permeate through empty space rather than polarizable media. This manifests itself as a position-dependent (nonlocal) dielectric response and the simple r^{-1} interaction is replaced by the Rytova-Keldysh potential [21,22] that has a much weaker (i.e., logarithmic) divergence as $r \to 0$. Unfortunately, this model does not allow for analytical solutions and purely numerical or variational approaches are required [23–29].

Recently, Molas *et al.* [30] proposed a highly appealing alternative to the Rytova-Keldysh potential. They suggested replacing the bare Coulomb potential by a Kratzer form $-r^{-1} + Cr^{-2}$, where C is a positive constant. The repulsive core potential Cr^{-2} effectively captures the reduced binding at small electron-hole distances and was found to provide good agreement with measured exciton energies in various transition-metal dichalcogenides. Importantly, analytical eigenstates can readily be obtained in the Kratzer model. This opens a possibility of analyzing a wide range of perturbative properties of excitons such as the response to electric and magnetic fields analytically.

The response of low-dimensional excitons to electrostatic fields has been widely used to characterize and manipulate the states [31–33]. In the weak-field limit, the perturbation is captured by the exciton polarizability that is a sensitive measure of binding energy. Thus, highly screened excitons are easily polarized resulting in a huge enhancement of the polarizability. In stronger fields, excitons may even dissociate into free electrons and holes before recombining [26]. The lack of analytical solutions in the Rytova-Keldysh model has meant that previous studies of static and dynamic polarizabilities have all been purely numerical [23–28]. While highly accurate, such calculations are computationally demanding and simple physical insight, such as parameter dependence, can be hard to extract. In the present work, we analyze the weak-field Stark problem for low-dimensional nonhydrogenic excitons described by the Kratzer potential. We profit greatly from the analytical eigenstates and demonstrate that analytical electric dipole polarizabilities can be computed for arbitrary values of the repulsive core. Moreover, our results are not restricted to two dimensions but apply to any dimension $D \geqslant 2$, even noninteger ones. We also compute bound-bound and bound-continuum oscillator strengths allowing for accurate dynamical polarizabilities. We restrict our analysis to static and dynamic polarizabilities of excitons in the 1*s* ground state since these are normally of greatest experimental relevance. However, the developed approach could be applied to excited states as well.

———————
*tgp@mp.aau.dk

II. SCREENED D-DIMENSIONAL EXCITONS

We consider excitons in a D-dimensional semiconductor with background dielectric screening through a dielectric constant ε. Thus, in three dimensions, ε represents the screening of the semiconductor itself, while in two dimensions, ε is the average of dielectric constants above and below the sheet. Throughout, we use "exciton" units, which generalize atomic units to problems with dielectric constant ε and reduced mass $m_e m_h / (m_e + m_h) \equiv \mu m_0$, where $m_{e/h}$ are effective electron/hole masses and m_0 is the free electron mass. Thus, we measure distances and energies in units of effective Bohr radii $a_0^* = (\varepsilon/\mu)a_0$ and effective hartrees $Ha^* = \mu/\varepsilon^2 Ha$, where a_0 and Ha are the usual atomic quantities. Also, polarizabilities are given in units of $4\pi\varepsilon_0 a_0^3 e^4/\mu^2$. In physical units, the Kratzer potential suggested by Molas *et al.* [30] is

$$V(r) = -\frac{e^2}{4\pi\varepsilon\varepsilon_0}\left(\frac{1}{r} - \frac{g^2 r_0}{\varepsilon r^2}\right). \tag{1}$$

Here, r_0 is the screening length of the two-dimensional (2D) semiconductor and $g \approx 0.21$ is an empirical parameter adjusted to fit the Keldysh potential. In exciton units, the potential can be written

$$V(r) = -\frac{1}{r} + \frac{\beta^2}{2r^2}. \tag{2}$$

The important factor $\beta^2 = 2\mu g^2 r_0/(\varepsilon^2 a_0)$ governs the strength of the repulsive core and the potential minimum is located at $r = \beta^2$. Numerically, taking MoS_2 ($\mu = 0.28$ and $r_0 = 44.3$ Å) and WSe_2 ($\mu = 0.23$ and $r_0 = 46.2$ Å) parameters [34], we find $\beta_{MoS_2} \approx 2.72/\varepsilon$ and $\beta_{WSe_2} \approx 2.78/\varepsilon$. Since typical dielectric constants are in the range $1 \leqslant \varepsilon \leqslant 10$, we see that relevant values of β are of order unity. As an alternative to fitting the potential, β can be determined by requiring a match to the $1s$ exciton binding energy. In the Keldysh model, a highly accurate fit is $E_{1s} \approx -2/(1 + a\tilde{r}_0^p)$, where $a \approx 2.64$, $p \approx 0.712$, and $\tilde{r}_0 = \mu r_0/\varepsilon^2$ is an effective screening length [24]. As we show below, in the two-dimensional Kratzer model $E_{1s} = -2/(1 + 2\beta)^2$ and, hence, matching means $\beta \approx \frac{1}{2}[(1 + a\tilde{r}_0^p)^{1/2} - 1]$. In fact, we find that Kratzer and Keldysh models are in significantly better agreement if this last fixing of β is adopted. Hence, in the numerical results below, we take $\beta_{MoS_2} \approx \frac{1}{2}[(1 + 25.0/\varepsilon^{2p})^{1/2} - 1]$ and $\beta_{WSe_2} \approx \frac{1}{2}[(1 + 22.4/\varepsilon^{2p})^{1/2} - 1]$. In Fig. 1, the Kratzer potential is sketched including the tilt inflicted by a static electric field in the Stark problem.

In a general "central" potential, the D-dimensional Hamiltonian is [10–15]

$$H_0 = -\frac{1}{2}\frac{d^2}{dr^2} - \frac{D-1}{2r}\frac{d}{dr} + \frac{\hat{l}^2}{2r^2} + V(r). \tag{3}$$

Here, $\hat{l}^2$ is the square of the angular momentum with eigenstates $\Theta_l(\theta)$ obeying $\hat{l}^2\Theta_l(\theta) = l(l + D - 2)\Theta_l(\theta)$ with l integer and θ the polar angle. We first discuss the unperturbed s and p states with $l = 0$ and 1, respectively, since these are involved in the ground state Stark problem. To this end, we introduce the exponents $\gamma = 1 + \sqrt{\beta^2 + (D/2 - 1)^2}$ and $\lambda = \sqrt{\beta^2 + (D/2)^2}$ as well as wave numbers $k_n^{(s)} = 2/(2n - 3 + 2\gamma)$ and $k_n^{(p)} = 2/(2n - 3 + 2\lambda)$, where n is an integer starting
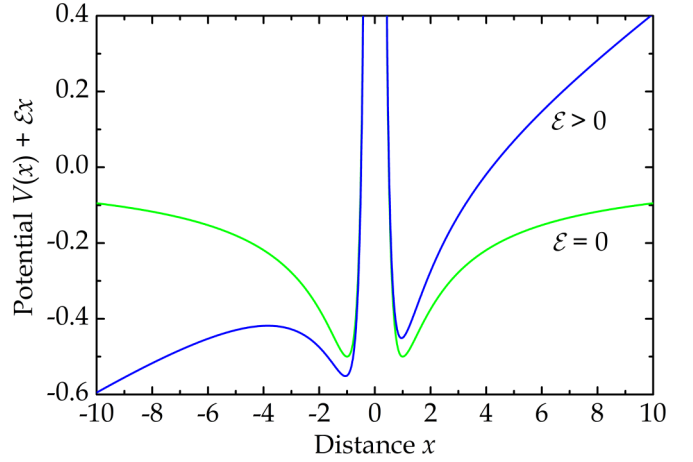

FIG. 1. Kratzer potential taking $\beta = 1$ in the absence and presence of an electric field $\mathcal{E}$.

at $n = 1$ and $n = 2$ for s and p states, respectively. These wave numbers determine energies $E_{ns/p} = -(k_n^{(s/p)})^2/2$ as well as radial eigenstates [35]

$$R_{ns}(r) = \left(2k_n^{(s)}\right)^{\gamma+1/2} e^{-k_n^{(s)}r} r^{\gamma-D/2}\sqrt{\frac{(n-1)!}{4\Gamma(n-2+2\gamma)}}$$
$$\times L_{n-1}^{2\gamma-2}\left(2k_n^{(s)}r\right), \tag{4}$$

and

$$R_{np}(r) = \left(2k_n^{(p)}\right)^{\lambda+3/2} e^{-k_n^{(p)}r} r^{\lambda+1-D/2}\sqrt{\frac{(n-2)!}{4\Gamma(n-1+2\lambda)}}$$
$$\times L_{n-2}^{2\lambda}\left(2k_n^{(p)}r\right). \tag{5}$$

These functions are normalized according to the D-dimensional radial measure $r^{D-1}dr$. An immediate application of these analytic expressions is a simple result for the mean square radius $\langle r^2 \rangle_{ns/p} = \int_0^\infty R_{ns/p}^2(r) r^{D+1} dr$, which reads for s and p states

$$\langle r^2 \rangle_{ns} = \frac{(2-\gamma)(5-2\gamma) + 5n(n-3+2\gamma)}{2\left(k_n^{(s)}\right)^2},$$
$$\langle r^2 \rangle_{np} = \frac{(1-\lambda)(13-2\lambda) + 5n(n-3+2\lambda)}{2\left(k_n^{(p)}\right)^2}. \tag{6}$$

These expressions are valid in arbitrary dimensions D and describe the diamagnetic shift of 2D semiconductors in a perpendicular magnetic field. For the ground state, we use the special notation $k_D \equiv k_1^{(s)} = 2/(2\gamma - 1)$ so that

$$R_{1s}(r) = \frac{(2k_D)^\gamma}{\sqrt{\Gamma(2\gamma)}} r^{\gamma-D/2} e^{-k_D r}. \tag{7}$$

In addition, the unperturbed ground state energy is $E_{1s} = -k_D^2/2 = -2/(2\gamma - 1)^2$. Hence, in two dimensions, $\gamma = 1 + \beta$ and $E_{1s} = -2/(1 + 2\beta)^2$.

III. EXACT DALGARNO-LEWIS POLARIZABILITY

We now include a static electric field $\mathcal{E}$ directed along an unconfined direction, i.e., parallel to the semiconductor

sheet in the two-dimensional case. In polar coordinates, the interaction is $\mathcal{E}r\cos\theta$ so that the full problem reads

$$\{H_0 + \mathcal{E}r\cos\theta\}\varphi(r,\theta) = E\varphi(r,\theta). \qquad (8)$$

Various ways of attacking this problem exist. Traditionally, by expanding the perturbed wave function in a basis of unperturbed ones, the polarizability is expressed as a sum over transitions between ground and excited states weighted by oscillator strengths. We follow this approach in the time-dependent case in the next section. However, in the case of a static electric field, the Dalgarno-Lewis approach [36–39] is advantageous. This method bypasses the complicated sum over states in the traditional approach, which, incidentally includes an involved integral over states whenever a continuum of excited states occurs, as in the present case. We previously [39] applied this approach to the related Stark effect in one-dimensional, one-sided Kratzer potentials $V(x)$ with $x \geqslant 0$. Briefly, the Dalgarno-Lewis approach proceeds by solving Eq. (8) order by order in the electric field. To this end, we expand $\varphi(r,\theta) = \varphi_0(r,\theta) + \mathcal{E}\varphi_1(r,\theta) + \mathcal{E}^2\varphi_2(r,\theta) + ...$ and similarly, $E(\mathcal{E}) = E_0 + \mathcal{E}^2 E_2 + ...$ Note that only even orders appear in the series for the energy in geometries that are inversion symmetric in the absence of the field. In the case of the ground state, we write $\varphi_1(r,\theta) = \cos\theta\, f(r)R_{1s}(r)$, such that f obeys the inhomogeneous equation

$$\left\{-\frac{1}{2}\frac{d^2}{dr^2} - \frac{D-1}{2r}\frac{d}{dr} + \frac{D-1}{2r^2} - \frac{R'_{1s}(r)}{R_{1s}(r)}\frac{d}{dr}\right\}f(r) + r = 0. \qquad (9)$$

Upon solving, the polarizability $\alpha_D = -2E_2$ is given by

$$\alpha_D = -\frac{2}{D}\int_0^\infty R_{1s}^2(r)f(r)r^D dr. \qquad (10)$$

The first-order problem, Eq. (9), is relatively complicated and obtaining a solution requires some effort. However, a homogeneous solution $f_H(r)$ containing a $_1F_1$ hypergeometric

function is readily found, i.e.,

$$f_H(r) = r^{1-\gamma+\lambda}{}_1F_1[1-\gamma+\lambda, 1+2\lambda, 2k_D r] \qquad (11)$$

A particular solution to Eq. (9) is harder to find. Our brute-force approach relies on the fact that it may be shown that the following series is a solution:

$$f_P(r) = r^3\sum_{n=0}^\infty a_n r^n, \quad a_0 = \frac{2}{4+6\gamma-D},$$

$$a_n = \frac{2k_D(n+2)}{(n+2+\gamma)^2 - \lambda^2}a_{n-1}. \qquad (12)$$

Because of the simple form of the recursive relation between a_n and a_{n-1}, a general solution can be found:

$$a_n = \frac{\Gamma(n+3)\Gamma(3+\gamma-\lambda)\Gamma(3+\gamma+\lambda)(2k_D)^n}{\Gamma(3+n+\gamma-\lambda)\Gamma(3+n+\gamma+\lambda)(4+6\gamma-D)}. \qquad (13)$$

It then turns out that the sum in Eq. (12) can be performed analytically with a result given in terms of a $_3F_2$ hypergeometric function

$$f_P(r) = \frac{2r^3}{4+6\gamma-D}{}_2F_2[1, 3, 3+\gamma-\lambda, 3+\gamma+\lambda, 2k_D r]. \qquad (14)$$

Both homogeneous and particular solutions diverge as $r \to \infty$. Hence, the full solution $f(r) = f_P(r) - Nf_H(r)$ must be constructed such that the divergences cancel with the result

$$N = \frac{\Gamma(1-\gamma+\lambda)\Gamma(3+\gamma-\lambda)\Gamma(3+\gamma+\lambda)}{(2k_D)^{2+\gamma-\lambda}(4+6\gamma-D)\Gamma(1+2\lambda)}. \qquad (15)$$

In this manner, a complete solution to Eq. (9) valid for arbitrary D and β is found.

Next, the problem of performing the integral in Eq. (10) must be tackled. A straightforward insertion of Eqs. (11) and (14) is problematic because both contributions diverge individually. Fortunately, using integral representations of both hypergeometrics, it can be shown that

$$\alpha_D = \frac{\gamma(1+\gamma)(1+2\gamma)(3+2\gamma)(\gamma+\lambda)(1+\gamma+\lambda)(2+\gamma-\lambda)}{2Dk_D^4(4+6\gamma-D)}\int_0^1 (t-1)^2 t^{\gamma+\lambda-1}{}_2F_1[1, 4+2\gamma, 3+\gamma+\lambda, t]dt \qquad (16)$$

In this form, both contributions are included leading to a cancellation of divergences. Finally, in terms of another $_3F_2$ hypergeometric function,

$$\alpha_D = \frac{\gamma(1+\gamma)(1+2\gamma)(3+2\gamma)(\gamma+\lambda)(1+\gamma+\lambda)(2+\gamma-\lambda)}{Dk_D^4(4+6\gamma-D)(1-\gamma+\lambda)(3+\gamma+\lambda)(4+\gamma-\lambda)}{}_3F_2[3, 3, 1-\gamma+\lambda, 2-\gamma+\lambda, 5+\gamma+\lambda, 1] \qquad (17)$$

This important closed-form expression is an exact formula for the polarizability valid in arbitrary dimensions D and repulsive core potentials β.

It is interesting to study the behavior of α_D in the limit $\beta \to 0$. This means taking somewhat involved limits of hypergeometric functions, the details of which are found in the Appendix. Using these results, in $D > 2$,

$$\alpha_D = \frac{(D-1)^4(D+1)(2D+3)}{128} + \frac{(D-1)^3(32D^3+49D^2+6D-7)}{128D(D-2)}\beta^2$$

$$+ (D-1)^2\left\{\frac{F(D)}{128(D-2)^3D^3(D+2)^2(D+3)^2} + \frac{(D^2-1)^2\psi^{(1)}(D+4)}{64(D-2)^2D}\right\}\beta^4 + O(\beta^6) \qquad (18)$$

with

$$F(D) = 190D^{10} + 1581D^9 + 3481D^8 - 3698D^7$$
$$- 22972D^6 - 24199D^5 + 833D^4 + 9140D^3$$
$$+ 1396D^2 - 168D - 144. \qquad (19)$$

This result breaks down in $D = 2$, but separate evaluation using the correct form in Eq. (A1) shows that

$$\alpha_2 = \frac{21}{128} + \frac{457}{256}\beta + \frac{2084 + 3\pi^2}{256}\beta^2 + O(\beta^3). \qquad (20)$$

In $D = 3$, Eq. (18) becomes

$$\alpha_3 = \frac{9}{2} + \frac{329}{12}\beta^2 + \frac{1539 + 8\pi^2}{36}\beta^4 + O(\beta^6). \qquad (21)$$

The $\beta = 0$ values in Eqs. (18), (20), and (21) agree perfectly with previous results [15,16,37]. It is also clear from the numerical values of the dominating corrections, i.e., $457\beta/256$ in two dimensions and $329\beta^2/12$ in three dimensions, that even relatively small values of β should imply huge corrections to the polarizability. In the opposite limit of large $\beta \gg 1$, we find from Eq. (A3)

$$\alpha_D = \frac{4}{D(D-1)}\beta^8 + \frac{18}{D(D-1)}\beta^7$$
$$+ \frac{41 - 7D + 4D^2}{D(D-1)}\beta^6 + O(\beta^5). \qquad (22)$$

Thus, an extremely rapid increase in polarizability is observed as $\beta \to \infty$. In Fig. 2, we plot the evolution of α_D with increasing β for three characteristic dimensions $D = 2, 2.5,$ and 3. Here, noninteger dimensions should be viewed as a device for interpolation between integer values. Thus, $D = 2.5$ emulates a finite-width quantum well [12,13] as opposed to a "zero-width" ideal quantum well. In each plot, the asymptotic expansions Eqs. (18), (20), and (22) are included. The asymptotic results are seen to be in excellent agreement with exact ones in the appropriate limits. In fact, simple addition of small- and large-β expansions leads to a good global approximation, as is easily checked. In all cases, it is clear that core potential strengths of $\beta \sim 1$ implies polarizabilities increased by one to two orders of magnitude compared to hydrogenic $\beta = 0$ values.

IV. OSCILLATOR STRENGTHS AND DYNAMIC POLARIZABILITY

The previous section demonstrated that Dalgarno-Lewis perturbation theory provides analytical, closed-form results for the static polarizability. In the dynamic case, however, the need to solve time-dependent perturbation problems renders analytical expressions highly nontrivial, although closed-form exact results for $\beta = 0$ but arbitrary D have recently been found [17]. As a feasible semianalytical alternative we opt to compute analytical oscillator strengths, which are subsequently summed numerically. Thus, for an electric field oscillating with frequency ω, the dynamic polarizability is
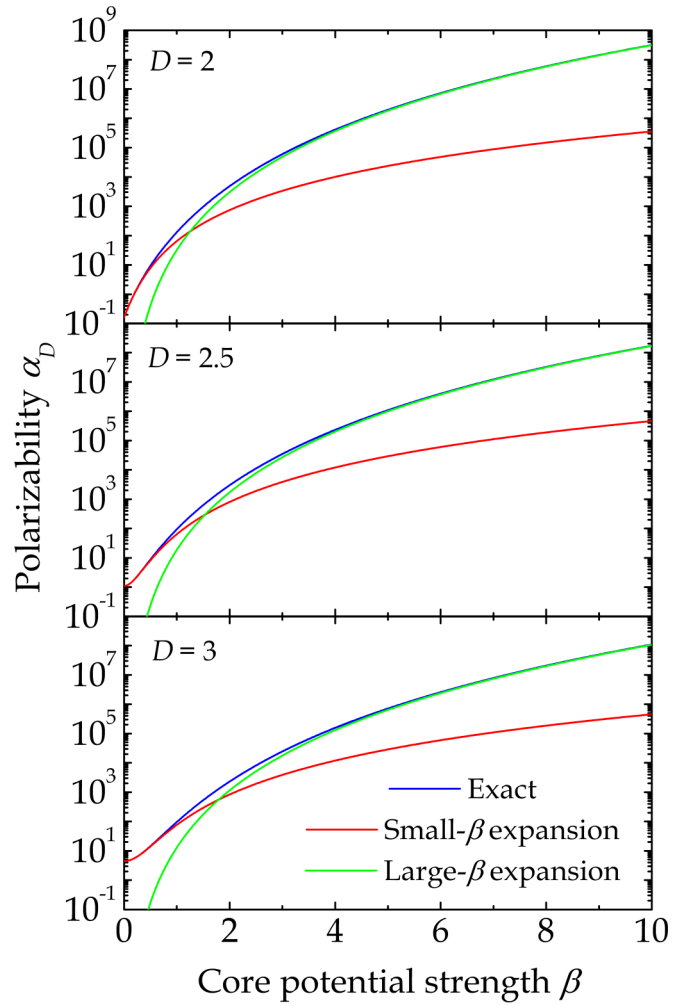

FIG. 2. Static polarizabilities of D-dimensional excitons versus core potential. Exact results (blue curves) are compared to $O(\beta^5)$ expansions (red curves) as well as asymptotic large-β limits (green curves).

obtained from the formula

$$\alpha_D(\omega) = \sum_n \frac{g_D(n)}{(E_{np} - E_{1s})^2 - \omega^2}$$
$$+ \int_0^\infty \frac{g'_D(k)}{(E_{kp} - E_{1s})^2 - \omega^2}dk. \qquad (23)$$

Here, $g_D(n) = 2(E_{np} - E_{1s})|\langle \varphi_{np}|r\cos\theta|\varphi_{1s}\rangle|^2$ is the bound-bound oscillator strength. Similarly, the second term in Eq. (23) contains bound-continuum contributions involving continuum p states with energy $E_{kp} = k^2/2$ and radial part

$$R_{kp}(r) = \frac{(2k)^{\lambda+1/2}\Gamma\left(\frac{1}{2} + \frac{i}{k} + \lambda\right)e^{\pi/2k}}{2\sqrt{\pi}\Gamma(1 + 2\lambda)}e^{-ikr}r^{1+\lambda-D/2}$$
$$\times \, _1F_1\left[\frac{1}{2} + \frac{i}{k} + \lambda, 1 + 2\lambda, 2ikr\right] \qquad (24)$$

For bound-bound transitions $1s \rightarrow np$, the oscillator strength becomes

$$g_D(n) = \frac{4^{\gamma+\lambda}2\Gamma(2+\gamma+\lambda)^2\Gamma(n-1+2\lambda)(k_D+k_n^{(p)})k_D^{2\gamma}(k_n^{(p)})^{3+2\lambda}}{D\Gamma(2\lambda)\Gamma(1+2\lambda)^2(n-2)!(k_D-k_n^{(p)})^{3+2\gamma+2\lambda}}\left|{}_2F_1\left[2+\gamma+\lambda, n-1+2\lambda, 1+2\lambda, \frac{2k_n^{(p)}}{k_n^{(p)}-k_D}\right]\right|^2 \quad (25)$$

Similarly, the bound-continuum $1s \rightarrow kp$ oscillator strength is

$$g'_D(k) = \frac{e^{\pi/k}4^{\gamma+\lambda}\Gamma(2+\gamma+\lambda)^2k_D^{2\gamma}k^{1+2\lambda}}{\pi D\Gamma(2\lambda)\Gamma(1+2\lambda)^2(k_D^2+k^2)^{1+\gamma+\lambda}}\left|\Gamma\left(\frac{1}{2}+\lambda+\frac{i}{k}\right){}_2F_1\left[2+\gamma+\lambda, \frac{1}{2}+\lambda+\frac{i}{k}, 1+2\lambda, \frac{2ik}{k_D+ik}\right]\right|^2 \quad (26)$$

The oscillator strengths satisfy the Thomas-Reiche-Kuhn [40,41] sum rule $S_0 = 1$, where S_p is the pth transition energy moment of the oscillator strength

$$S_p = \sum_n g_D(n)(E_{np}-E_{1s})^p + \int_0^\infty g'_D(k)(E_{kp}-E_{1s})^p dk. \quad (27)$$

Several other moments can be found from matrix elements of the ground state only [42] and some characteristic important cases are

$$S_{-2} = \alpha_D, \quad S_{-1} = \frac{\gamma(1+2\gamma)(1-2\gamma)^2}{4D},$$

$$S_0 = 1, \quad S_1 = 4\frac{(D-2)^2+2(\gamma-1)}{D(1-\gamma)(1-2\gamma)^3},$$

$$S_2 = 16\frac{12+8D^2-D^3-2D(10-\gamma)+2\gamma(1-2\gamma)}{D(2-\gamma)(1-\gamma)(3-2\gamma)(1-2\gamma)^5}. \quad (28)$$

These relations have all been verified numerically. Also, in Fig. 3, the dominant oscillator strengths are shown versus core potential β. The plot includes the summed bound-bound contributions $\sum_n g_D(n)$ that, it should be stressed, do not equal unity because bound-continuum contributions are omitted. However, irrespective of dimension, the sum $\sum_n g_D(n)$ is seen to approach unity as β increases. Importantly, the lowest transition $1s \rightarrow 2p$ oscillator strength $g_D(2)$ increases dramatically with β initially and reaches a maximum $g_D(2) \geqslant 0.95$ around $\beta \sim 1$–2, which coincides with the physically relevant range. This means that this single transition is completely dominating in this range. In cases of larger β, the $1s \rightarrow 2p$ transition loses intensity, while $1s \rightarrow 3p$, in particular, gains intensity. It is interesting that, apparently, a characteristic (D-dependent) value of β can be found, at which $g_D(n) \approx 0$ for all $n > 2$.

We now turn to the dynamic polarizability given by Eq. (23) and illustrated in Fig. 4. Note that, in this plot, the frequency ω is actually the photon energy $\hbar\omega$ in natural exciton hartree units Ha*. Also, an imaginary part $i0.002k_D$ is added to the frequency to regularize divergencies at resonance. Below, results converted into physical units are provided as well. From Fig. 4 it is seen that discrete bound-bound transitions contribute by amounts that decrease with transition energy. Thus, $1s \rightarrow 3p$ transitions are always significantly less intense than $1s \rightarrow 2p$ transitions. Moreover, the $\beta = 0$ and $\beta = 0.1$ cases are seen to be qualitatively quite similar except for the compressed energy range in the latter case. In contrast, the more realistic $\beta = 1$ case differs by featuring a

nonmonotonic D dependence of $1s \rightarrow np$ transition energies. In fact, at $\beta = 1$, the two-dimensional case has the lowest $1s \rightarrow 2p$ resonance, in stark contrast to the hydrogenic model. Finally, it is observed that the overall intensity of the spectra increases significantly with β.

We finish this section by presenting polarizability spectra for real two-dimensional transition-metal dichalcogenides obtained by converting normalized quantities into physical values. To this end, we consider suspended ($\varepsilon = 1$) and hexagonal boron nitride (hBN) encapsulated ($\varepsilon = 4.9$)
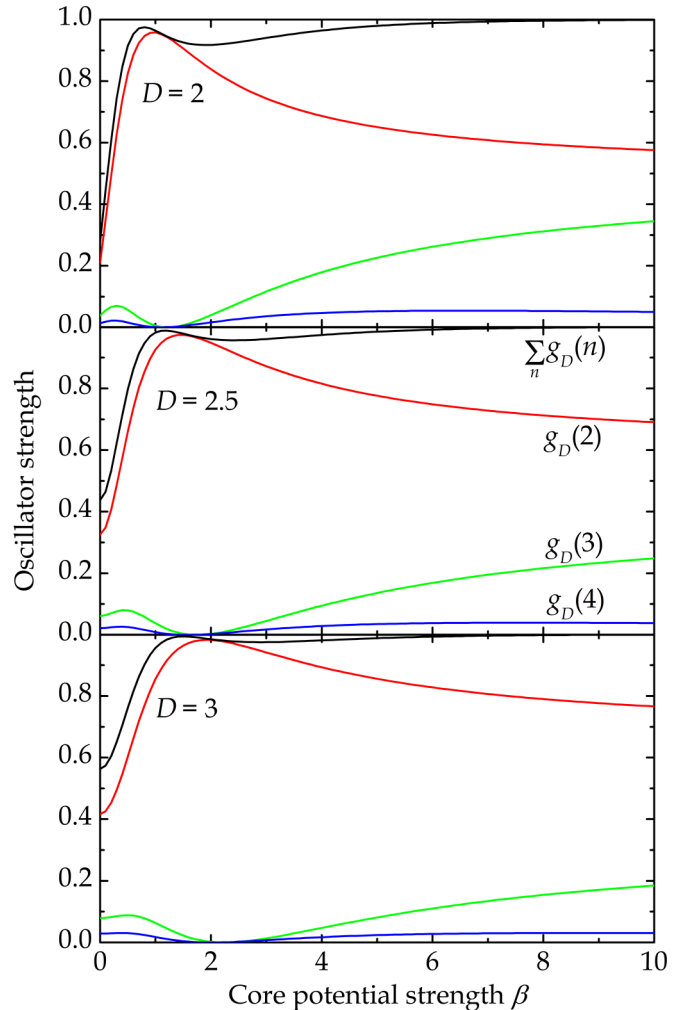

FIG. 3. Oscillator strengths of the three lowest bound-bound transitions versus β. The black curves illustrate the sum of all bound-bound contributions.
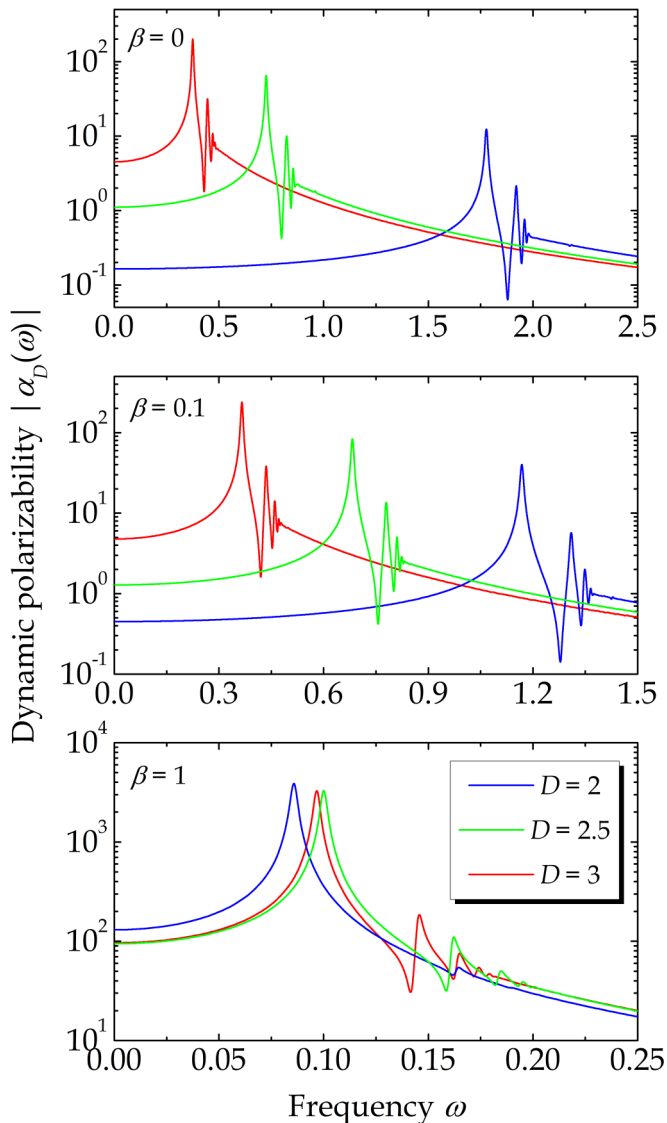
FIG. 4. Dynamic polarizability of low-dimensional excitons in various dimensions as indicated by color. The three panels show cases of vanishing (top panel), weak (middle panel), and realistic (bottom panel) core potentials.

FIG. 5. Dynamic polarizability of MoS_2 and WSe_2 in different dielectric environments. The $1s \rightarrow np$ transition energies are indicated by colored bars.

static polarizability is in reasonable agreement with numerical Keldysh values. In Ref. [24], the polarizabilities of freely suspended MoS_2 and WSe_2 were determined to be 4.6×10^{-18} and $6.3 \times 10^{-18} eV(m/V)^2$, respectively. The corresponding values in the present Kratzer model are both approximately $7.3 \times 10^{-18} eV(m/V)^2$. The approximately identical values for two different materials result from an accidental cancellation of effects due to r_0 and μ. In contrast, the Kratzer polarizabilities in screened ($\varepsilon = 4.9$) environments are substantially different from their Keldysh counterparts [24]. In fact, the static Kratzer polarizability decreases with ε, in marked contradiction to Keldysh values and physical intuition. Mathematically, this is a consequence of β decreasing rapidly as ε increases. This occurs irrespective of whether β is determined by matching to potential or exciton binding energy. In fact, in physical units, α_D as a function of ε goes through a minimum and eventually increases as ε becomes sufficiently large. Such behavior is presumably an unphysical artifact of the Kratzer model. Unfortunately, measurements in favor of either model do not exist as systematic experimental studies of exciton polarizabilities in different dielectric environments are still lacking.

V. SUMMARY

In summary, we have adopted the recently proposed Kratzer model to study Stark effects in nonhydrogenic excitons in low-dimensional semiconductors. The model incorporates position-dependent dielectric screening by including a repulsive core potential, yet remains analytically solvable in arbitrary dimensions. The perturbation by static

materials. For MoS_2, the corresponding core potentials are $\beta = 2.04$ and $\beta = 0.448$, while for WSe_2 we find $\beta = 1.92$ and $\beta = 0.412$, respectively. The dynamic polarizability spectra are shown in Fig. 5 including $1s \rightarrow np$ transition energies indicated by bars. In both MoS_2 and WSe_2, the dominating $1s \rightarrow 2p$ resonance is close to $\hbar\omega = 0.1$eV, irrespective of screening. In the screened cases, the bound-bound spectral range is greatly compressed, however, with a $1s$ ionization energy (i.e., negative of the $1s$ binding energy) around 0.17 eV. In contrast, the $1s$ ionization energy is 0.58 and 0.54 eV in suspended MoS_2 and WSe_2, respectively. These values are naturally in perfect agreement with Keldysh results [24] as this is precisely the requirement applied to fix β.

Turning to the polarizability spectra, the individual contributions to the full response are readily resolved and a smooth transition to the continuum regime at the dissociation threshold $\hbar\omega = |E_{1s}|$ is observed. The magnitude of the
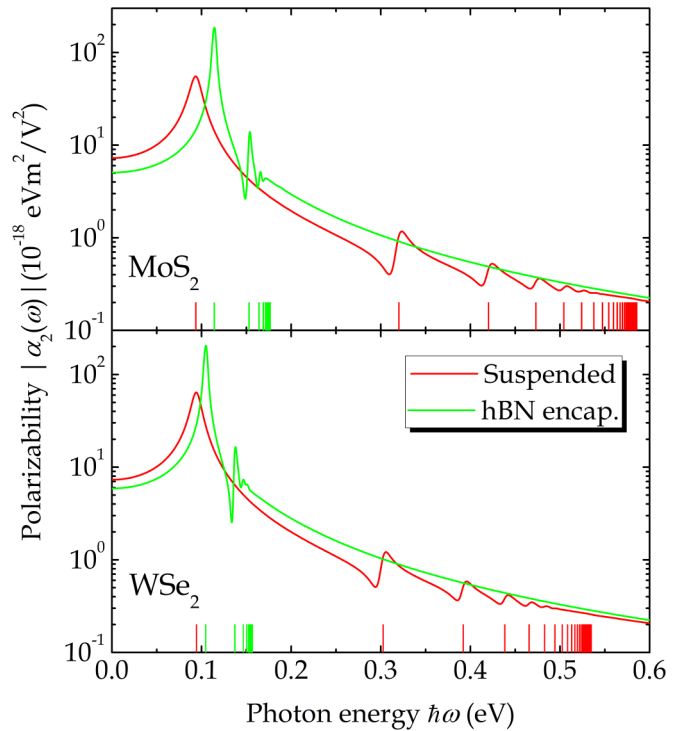
electric fields is handled analytically using the Dalgarno-Lewis approach. In turn, an exact expression for the static polarizability valid for arbitrary core potential strength and dimension is obtained. Moreover, analytical oscillator strengths of both bound-bound and bound-continuum transitions are derived, allowing for simple computations of the dynamic polarizability.

APPENDIX: LIMITING BEHAVIOR

In this Appendix, we derive expansions required to explain the behavior of α_D in the extreme limits $\beta \to 0$ and $\beta \to \infty$. In the former case, we see that

$$
-\gamma + \lambda = \begin{cases} -\frac{2\beta^2}{(D-2)D} + \frac{2(4-6D+3D^2)}{(D-2)^3 D^3}\beta^4 + O(\beta^6), & D > 2 \\ -\beta + \frac{\beta^2}{2} - \frac{\beta^4}{8} + O(\beta^6), & D = 2 \end{cases}.
$$

(A1)

In the opposite limit $\beta \to \infty$, i.e., the case of a dominating repulsive core, we find $1 - \gamma + \lambda = (D-1)[\frac{1}{2}\beta^{-1} - \frac{1}{16}(2-2D+D^2)\beta^{-3} + O(\beta^{-5})]$ valid in any dimension. Hence, in both limits, we may expand Eq. (17) since $-\gamma + \lambda$

approaches an integer. In practice, one writes the $_3F_2$ hypergeometric function as an infinite sum over Pochhammer symbol ratios, expands each term in the sum, and finally re-sums the result order by order. The final expressions for the required expansions can be written as

$$
_3F_2[3, 3, 1 + x, 2 + x, 5 + y, 1]
$$

$$
= \frac{(4+y)(3+2y)}{2y(1+y)} + \frac{(4+y)(36+37y+9y^2)}{4y(1+y)(2+y)(3+y)}x
$$

$$
+ \frac{4+y}{4}\left\{\psi^{(1)}(4+y) - \frac{5+y}{(1+y)(3+y)}\right\}x^2 + O(x^3)
$$

(A2)

and

$$
_3F_2[3, 3, x, 1 + x, 5 + y, 1]
$$

$$
= 1 + \frac{(8+3y)(18+16y+3y^2)}{y(2+y)(3+y)(4+y)}x - \left\{\psi^{(1)}(5+y)\right.
$$

$$
\left. + \frac{176+257y+115y^2+16y^3}{2(1+y)(2+y)(3+y)(4+y)}\right\}x^2 + O(x^3), \quad \text{(A3)}
$$

where $\psi^{(1)}(z) = d^2 \ln \Gamma(z)/dz^2$ is the trigamma function.

[1] H. Haug and S. W. Koch, *Quantum Theory of the Optical and Electronic Properties of Semiconductors* (World Scientific, Singapore, 1993).

[2] P. K. Basu, *Theory of Optical Processes in Semiconductors* (Oxford University Press, Oxford, 1997).

[3] T. Mueller and E. Malic, npj 2D Mater. Appl. **2**, 29 (2018).

[4] A. Ramasubramaniam, Phys. Rev. B **86**, 115409 (2012).

[5] D. Y. Qiu, F. H. da Jornada, and S. G. Louie, Phys. Rev. Lett. **111**, 216805 (2013).

[6] S. Latini, T. Olsen, and K. S. Thygesen, Phys. Rev. B **92**, 245123 (2015).

[7] G. H. Wannier, Phys. Rev. **52**, 191 (1937).

[8] Y. Shinozuka and M. Matsuura, Phys. Rev. B **28**, 4878 (1983).

[9] T. Olsen, S. Latini, F. Rasmussen, and K. S. Thygesen, Phys. Rev. Lett. **116**, 056401 (2016).

[10] M. Florian, M. Hartmann, A. Steinhoff, J. Klein, A. W. Holleitner, J. J. Finley, T. O. Wehling, M. Kaniber, and C. Gies, Nano Lett. **18**, 2725 (2018).

[11] M. O. Sauer, Carl Emil Morch Nielsen, L. Merring-Mikkelsen, and T. G. Pedersen, Phys. Rev. B **103**, 205404 (2021).

[12] X-F. He, Phys. Rev. B **43**, 2063 (1991).

[13] P. Lefebvre, P. Christol, and H. Mathieu, Phys. Rev. B **48**, 17308 (1993).

[14] T. F. Rønnow, T. G. Pedersen, and B. Partoens, Phys. Rev. B **85**, 045412 (2012).

[15] T. G. Pedersen, H. Mera, and B. K. Nikolić, Phys. Rev. A **93**, 013409 (2016).

[16] T. G. Pedersen, Solid State Commun. **141**, 569 (2007).

[17] T. G. Pedersen, Phys. Rev. B **104**, 155414 (2021).

[18] G. M. Kavoulakis, Y.-C. Chang, and G. Baym, Phys. Rev. B **55**, 7593 (1997).

[19] A. Chernikov, T. C. Berkelbach, H. M. Hill, A. Rigosi, Y. Li, B. Aslan, D. R. Reichman, M. S. Hybertsen, and T. F. Heinz, Phys. Rev. Lett. **113**, 076802 (2014).

[20] Z. Ye, T. Cao, K. O'Brien, H. Zhu, X. Yin, Y. Wang, S. G. Louie, and X. Zhang, Nature (London) **513**, 214 (2014).

[21] N. S. Rytova, Moscow Univ. Bull., Ser. 3 (Engl. Transl.) **3**, 30 (1967).

[22] L. V. Keldysh, JETP Lett. **29**, 658 (1978).

[23] S. Haastrup, S. Latini, K. Bolotin, and K. S. Thygesen, Phys. Rev. B **94**, 041401(R) (2016).

[24] T. G. Pedersen, Phys. Rev. B **94**, 125424 (2016).

[25] B. Scharf, T. Frank, M. Gmitra, J. Fabian, I. Žutić, and V. Perebeinos, Phys. Rev. B **94**, 245434 (2016).

[26] M. Massicotte, F. Vialla, P. Schmidt, M. Lundeberg, S. Latini, S. Haastrup, M. Danovich, D. Davydovskaya, K. Watanabe, T. Taniguchi, V. Fal'ko, K. Thygesen, T. G. Pedersen, and F. H. L. Koppens, Nat. Commun. **9**, 1633 (2018).

[27] L. S. R. Cavalcante, D. R. da Costa, G. A. Farias, D. R. Reichman, and A. Chaves, Phys. Rev. B **98**, 245309 (2018).

[28] M. N. Brunetti, O. L. Berman, and R. Ya. Kezerashvili, Phys. Rev. B **98**, 125406 (2018).

[29] M. F. C. M. Quintela, J. C. G. Henriques, L. G. M. Tenório, and N. M. R. Peres, Phys. Status Solidi B **259**, 2200097 (2022).

[30] M. R. Molas, A. O. Slobodeniuk, K. Nogajewski, M. Bartos, Ł. Bala, A. Babiński, K. Watanabe, T. Taniguchi, C. Faugeras, and M. Potemski, Phys. Rev. Lett. **123**, 136801 (2019).

[31] J. Klein, J. Wierzbowski, A. Regler, J. Becker, F. Heimbach, K. Müller, M. Kaniber, and J. J. Finley, Nano. Lett. **16**, 1554 (2016).

[32] J. G. Roch, N. Leisgang, G. Froehlicher, P. Makk, K. Watanabe, T. Taniguchi, C. Schönenberger, and R. J. Warburtonet, Nano Lett. **18**, 1070 (2018).

[33] I. Verzhbitskiy, D. Vella, K. Watanabe, T. Taniguchi, and G. Eda, ACS Nano **13**, 3218 (2019).

[34] F. A. Rasmussen and K. S. Thygesen, J. Phys. Chem. C **119**, 13169 (2015).

[35] S. M. Ikhdair and R. Sever, J. Math. Chem. **45**, 1137 (2009).

[36] A. Dalgarno and J. T. Lewis, Proc. R. Soc. London, Ser. A **233**, 70 (1955).

[37] T. G. Pedersen, S. Latini, K. S. Thygesen, H. Mera, and B. K. Nikolic, New J. Phys. **18**, 073043 (2016).

[38] T. G. Pedersen, Phys. Rev. A **99**, 063410 (2019).

[39] T. G. Pedersen, J. Phys. B: At. Mol. Phys. **53**, 175101 (2020).

[40] W. Kuhn, Z. Phys. **33**, 408 (1925).

[41] F. Reiche and W. Thomas, Z. Phys. **34**, 510 (1925).

[42] R. Jackiw, Phys. Rev. **157**, 1220 (1967).